

# **Cone dystrophy with “supernormal” rod ERG: psychophysical testing shows comparable rod and cone temporal sensitivity losses with no gain in rod function**

Andrew Stockman<sup>1</sup>, G. Bruce Henning<sup>1</sup>, Michel Michaelides<sup>2</sup>, Anthony T. Moore<sup>2</sup>, Andrew R. Webster<sup>2</sup>, Jocelyn Cammack<sup>1</sup> and Caterina Ripamonti<sup>1</sup>

<sup>1</sup>*UCL Institute of Ophthalmology, University College London, 11-43 Bath Street, London EC1V 9EL, England*

<sup>2</sup>*Moorfields Eye Hospital, City Road, London, EC1V 2PD, England*

## **ABSTRACT**

### **Purpose:**

We report a psychophysical investigation of five observers with the retinal disorder “cone dystrophy with supernormal rod ERG”, caused by mutations in the gene *KCNV2* that encodes a voltage-gated potassium channel found in rod and cone photoreceptors. We compare losses for rod- and for cone-mediated vision to further investigate the disorder and to assess whether the supernormal ERG is associated with any visual benefit.

### **Methods:**

L-cone, S-cone and rod temporal acuity (critical flicker fusion frequency—cff) was measured as a function of target irradiance; L-cone temporal contrast-sensitivity was measured as a function of temporal frequency.

### **Results:**

Temporal acuity measures reveal that losses for vision mediated by rods, S-cones and L-cones are roughly equivalent. Further, the gain in rod function implied by the supernormal ERG provides no apparent benefit to near-threshold rod-mediated visual performance. The L-cone temporal contrast-sensitivity function in affected observers is similar in shape to the mean normal function but only after the mean function has been compressed by halving the logarithmic sensitivities.

### **Conclusions:**

The name of this disorder is potentially misleading because the comparable losses found across rod and cone vision suggest that the disorder is a generalized cone-rod dystrophy. Temporal acuity and

temporal contrast-sensitivity measures are broadly consistent with the defect in the voltage-gated potassium channel producing a nonlinear distortion of the photoreceptor response but after otherwise normal transduction processes.

**Keywords:** Supernormal rod ERG, cone dystrophy, cone-rod dystrophies, flicker sensitivity, critical flicker fusion, temporal acuity, temporal processing, *KCNV2* gene.

## INTRODUCTION

The subject of this investigation is an unusual, autosomal recessive visual disorder, first described in 1983 in two siblings,<sup>1</sup> with a generalized and sometimes progressive loss of cone vision including reduced visual acuity, abnormal colour vision, photophobia and an attenuation of the cone ERG, all of which are consistent with cone dystrophy. A pathognomonic symptom, not associated with most other cone dystrophies, is that the rod b-wave is delayed and markedly reduced or absent at low flash intensities yet normal or “supernormal” in amplitude at the upper end of the scotopic region.<sup>2-8</sup> This electrophysiological enhancement has led to the disorder being referred to as “cone dystrophy with supernormal rod ERG” (CDSR).<sup>1</sup> Although electrophysiologically appropriate (but see Robson et al.<sup>9</sup>), the name of the disease seems strangely at odds with consistent reports, beginning with the initial description of the disease by Gouras et al.,<sup>1</sup> of night blindness (nyctalopia). Rod sensitivity losses of about 2 log<sub>10</sub> units have typically been reported.<sup>6-8</sup> Surprisingly, night blindness is not reported in some CDSR observers,<sup>9-12</sup> even in cases with reduced rod b-waves at low flash intensities. Subsequent to the initial report, the phenotype of this disorder has been the focus of several studies.<sup>2-10, 12</sup>

Our primary goal was to better characterize this disorder psychophysically under both scotopic (rod) and photopic (cone) conditions using standard behavioral assessments of temporal acuity measured as a function of light level. These measures allow us to compare the losses for rod- and cone-mediated vision. Are they similar, or are they more pronounced for cone-mediated vision? And, in particular, is there any visual advantage to the “supernormal” rod ERG response found at higher scotopic levels? One complication is that any progressive deterioration associated with the disease is likely to affect central cone-mediated vision more than peripheral rod-mediated vision.<sup>9, 13</sup> Yet any deficits due to the *KCNV2* mutation (as distinct from deficits resulting from progressive deterioration) should be more clearly apparent in rod sensitivity measurements.

Because the initial slope of ERG a-waves, which is receptorial in origin, is typically normal<sup>14, 15</sup> in CDSR, the deficit is reasonably assumed to arise after the transduction cascade, but before the inner nuclear layer.<sup>6-8</sup> More recently, sequence variants in the gene *KCNV2* have been found to underlie the disorder. *KCNV2* encodes a subunit of a voltage-gated potassium channel found in both rod and cone photoreceptors.<sup>11, 16-18</sup> Thus it has been suggested that the variants might affect the potassium current within photoreceptor inner segments.<sup>16</sup> Potassium channels in the inner segment are important for shaping the photoreceptor output response and setting the resting potential,<sup>19</sup> but precisely how defects in such channels might affect visual performance remains unclear. Our secondary goal was therefore to use psychophysical measures of cone temporal sensitivity to reveal more about the nature of the underlying molecular deficit. On the basis of previous findings we predicted that features of the temporal sensitivity functions that can be related to processes in the transduction cascade (such as activation and sensitivity regulation) would be relatively normal.<sup>20, 21</sup>

Our results suggest that the supernormal rod ERG response confers no benefit to rod-mediated visual performance in CDSR observers near threshold: rod-mediated visual performance seems as deficient as S- and L-cone-mediated performance, thus the disorder is consistent with a generalized cone-rod dystrophy. In light of this, we suggest renaming the disease “cone-rod dystrophy with supernormal rod ERG” (CRDSR), and we shall use this descriptor. One plausible interpretation of our measurements is that the mutant voltage-gated potassium channels attenuate and distort the cone response after transduction processes in the cone outersegment.

## METHODS

### *Subjects*

The experimental group of observers consisted of 5 individuals affected by CRDSR. The genotypes of the observers, with respect to the *KCNV2* gene, their gender and ages at the time of testing, and right and left eye acuities are as follows:

SR1	M	54	6/60 6/60	p.Lys3X homozygous
SR2	M	35	6/36 6/36	p.Gly306X homozygous
SR3	F	29	6/36, 6/36	c.1016_1024del, p.(Asp339_Val341del)
SR4	F	48	6/60, 6/60	p.Gly461Arg homozygous

Groups of adults with normal or corrected to normal visual acuity and normal colour vision provided representative control data. The normal observers all had normal colour vision as assessed by the Farnsworth-Munsell 100 hue test and other standard colour vision tests. Three of the supernormal rod ERG group also carried out the FM-100 test. All had low colour discriminations, but the axis of worst error varied: SR2 performed worst along a tritan/deutan axis (Total Error Score: 380), SR4 along a tritan/protan axis (TES: 219), and SR5 along a protan axis (TES: 248). These are consistent with the previous colour vision assessments of CRDSR observers referenced in the Introduction.

These studies conformed to the standards set by the Declaration of Helsinki, and the procedures have been approved by local ethics committees at Moorfields Eye Hospital and at University College London.

### ***Apparatus***

The psychophysical measurements were made using two standard, Maxwellian-view systems with 2-mm exit pupils. One system, used for the cone (photopic) experiments, was illuminated by a 900-W Xe arc lamp. The second system, used for the rod (scotopic) experiments, was illuminated by a 75-W Xe arc lamp. Both systems allow the projection of lights directly onto the observer's retina. The wavelengths of the target and background were selected by interference filters (Ealing or Oriel) with full bandwidth at half-maximum transmission of between 7 and 11-nm. The radiance in each channel was controlled by a combination of neutral-density filters (Oriel), and by the rotation, under computer control, of a circular, variable-neutral-density filter (Rolyn Optics).

Sinusoidal variation in the target radiance was produced by pulse-width modulation of the target beam by a fast, liquid-crystal, light shutter located in the target beam with rise and fall times faster than 50  $\mu$ s (Displaytech). The shutter was turned on and off at a fixed frequency of 400 Hz, but with a pulse-width that was varied sinusoidally under computer control using programmable timers (Data Translation, DT2819) to produce the sinusoidal stimuli at the desired *visible* frequencies and at signal modulations up to 92%. (Frequencies near the 400-Hz rectangular-pulse frequency and above were much too high to be resolved, so that observers saw only the sinusoidally-varying stimuli produced by the variation of the pulse-width.)

The position of the observer's head was maintained by a hardened dental wax impression mounted on a milling-machine head that could be adjusted in three dimensions to locate the exit

pupil of the optics in the centre, and in the plane of the observer's pupil. The system is described in full detail elsewhere.<sup>21-23</sup>

### **Stimuli**

The targets were sinusoidally flickered about a fixed mean radiance,  $\bar{R}$ . The flickering waveform,  $A(t)$ , is given by:

$$A(t) = \bar{R}\{1 + m \sin(2\pi ft)\}, \quad [1]$$

where  $f$  is the frequency of the flicker (in Hz), and  $m$  is the ripple ratio or "modulation", defined as the conventional Michelson contrast:

$$m = \frac{I_{max} - I_{min}}{I_{max} + I_{min}}. \quad [2]$$

$I_{max}$  and  $I_{min}$  are the maximum and minimum radiances of the stimulus, respectively. The modulation,  $m$ , could be varied under computer control, but was limited to a maximum of 92%. In the critical flicker fusion (cff) measurements the modulation was fixed at the maximum of 92%. In the modulation sensitivity measurements  $m$  was varied to find threshold.

*L-cone stimuli.* A flickering circular target of diameter  $4^\circ$  in visual angle and 650-nm in wavelength was presented in the centre of a  $9^\circ$  diameter background field of 481 nm. Fixation was central. The 481-nm background, which delivered  $8.29 \log \text{ quanta s}^{-1} \text{ deg}^{-2}$  at the cornea ( $1.42 \log_{10}$  photopic trolands or  $2.58 \log_{10}$  scotopic trolands), mainly served to suppress the rods, but also selectively desensitized the M-cones at lower target radiances. The primary target wavelength of 650-nm was chosen to favour detection by cones rather than rods. For the cff measurements, the target intensity was varied from 6.5 to  $11.5 \log_{10} \text{ quanta s}^{-1} \text{ deg}^{-2}$ . These conditions isolate the L-cone response over most of the 650-nm intensity range, but at high intensities the M-cones are also likely to contribute to flicker detection. For the modulation sensitivity measures the 650-nm target was fixed at a time-averaged radiance of  $10.28 \log \text{ quanta s}^{-1} \text{ deg}^{-2}$ .

*Rod stimuli.* A flickering target of  $5.74^\circ$  in diameter and 500-nm in wavelength was presented at an eccentricity of  $10^\circ$  in the temporal retina. Fixation was aided by a small red fixation light. No background was present. By convention, we use scotopic trolands (scot. td) for the rod measurements rather than quantal units. (To convert from  $\log_{10}$  scot. td to  $\log_{10} \text{ quanta s}^{-1} \text{ deg}^{-2}$  at 500-nm add 5.66 to the log troland values.) The intensity of the 500-nm target was increased in

steps from near absolute threshold (c.  $-4.25 \log \text{scot. td}$ ) to above cone threshold (c.  $2 \log \text{scot. td}$ ). The detection by cones at the highest levels was marked by an abrupt increase in cff. For two normal subjects, a control experiment was carried out and verified that the abrupt increase was due to cone detection by restricting measurements to the cone plateau that occurs over 3 and 10 minutes following an intense white bleach during which cones have recovered but rods have not (data not shown).<sup>24, 25</sup>

*S-cone stimuli.* A flickering target of  $4^\circ$  in diam. and 440-nm in wavelength was presented in the centre of a  $9^\circ$  diam. background field of 620 nm. Fixation was central. The 620-nm background radiance, fixed at  $11.41 \log_{10} \text{ quanta s}^{-1} \text{ deg.}^{-2}$  selectively desensitized the M- and L-cones, but had comparatively little direct effect on the S-cones. For normal observers, this field isolates the S-cone response to a 440-nm target up to a radiance of about  $10.0 \log_{10} \text{ quanta s}^{-1} \text{ deg.}^{-2}$ ; <sup>26-28</sup> above that radiance, the M-cones contribute to flicker detection. For the cff measurements, the 440-nm target radiance was varied from 6.30 to  $11.00 \log_{10} \text{ quanta s}^{-1} \text{ deg.}^{-2}$ .

### **Procedures**

Before every cone measurement, all observers light adapted to the background and target for 3 minutes. Before making any rod measurements, observers first dark-adapted in total darkness for 40 minutes.

The observers viewed the stimuli monocularly with their right eye unless they preferred to use their left eye and interacted with the computer that control the apparatus by means of an eight-button keypad. They received information and instructions via tones and a computer-controlled voice synthesizer. Each experiment was repeated three times usually on separate days. The mean of the results for each experimental run was averaged and the standard error determined. The visual stimulus, focused in the plane of the pupil, and the fixation light for the rod experiments, were the only visible light source for the observers in an otherwise dark room. The image of the source in the plane of the observers' pupils was always less than the minimal pupil size so that retinal illumination was not affected by pupil size. The method of adjustment was used to measure visual responses in the experiments.

Two types of experiments were performed.

*Critical flicker fusion measurements.* At each target radiance, observers adjusted the flicker frequency (at the fixed maximum stimulus modulation of 92%) to find the frequency at which the

flicker just disappeared—the critical fusion frequency or cff. The target radiance was increased from the lowest to highest radiances in steps of about  $0.3 \log_{10}$  unit for the cone measurements and about  $0.5 \log_{10}$  unit for the rod measurements. During a single run of the experiment, three settings were made at each radiance and averaged. The experimental runs were repeated on three separate occasions.

*Modulation sensitivity measurements.* The mean radiance of the 481-nm background and 650-nm target were fixed at 8.29 and 10.28 log quanta  $s^{-1} \text{ deg}^{-2}$ , respectively, and the frequency of the flickering target was fixed. Observers adjusted the modulation of the flickering stimulus ( $m$  in Equation 1) to determine the lowest modulation at which flicker was just visible. During a single run of the experiment, three settings were made at each radiance and flicker rate and then averaged. Then the frequency of the flicker was changed in 0.5-Hz steps from the lowest to the highest frequency that could be seen at the maximum modulation depth of 92%. The experimental runs were repeated on three separate occasions.

### **Calibration**

The radiant fluxes of the target and background fields were measured at the plane of the exit pupil using an UDT radiometer, calibrated by the manufacturer (Gamma Scientific) against a standard traceable to the US National Bureau of Standards. The neutral-density filters (and circular neutral-density wedge) were calibrated in the optical system, separately for each wavelength used, using the radiometer. All radiances are reported as time-averaged values.

## **RESULTS**

In all figures, data for the five CRDSR observers are distinguished as blue triangles (SR1), purple inverted triangles (SR2), green diamonds (SR3), yellow circles (SR4) and orange hexagons (SR5). The mean data for the five observers (or three in Figure 4) are shown by the grey dotted circles. Over the common ranges over which all observers could make settings (temporal frequencies in Figure 2, target irradiances in Figures 1, 3 and 4), the mean was obtained by simply averaging the individual data. Outside those ranges, the means were determined by first shifting the individual data on the vertical y-axis (in Hz for the cff measures or in log modulation units for the temporal contrast measurements) to align each observers data with the mean obtained from within the common range (using a least-squares fitting criterion). Then the aligned data were averaged to give the mean for

the data that lay outside the common range. This procedure avoided discontinuities due to individual observers' being unusually sensitive or insensitive. We note the best-fitting vertical shifts below, since they are of use in quantifying individual differences. The standard errors associated with the means were obtained from the *unshifted* individual data. The model fits described in the Discussion are fits to the unshifted data.

### ***L-cone critical flicker fusion***

Figure 1 shows L-cone cff (temporal acuity) data for the five observers affected by CRDSR plotted on a linear scale as a function of  $\log_{10}$  target radiance. The mean L-cone cff data for twelve observers with normal vision are plotted as red squares. The error bars in all figures are  $\pm 1$  standard error of the mean (s.e.m.) within observers for the individual CRDSR measurements, and between observers for the mean CRDSR data (grey circles) and mean normal measurements (red squares). The optimal least-squared shifts of the individual data required to vertically align with the mean (grey circles) over the common range of target radiances was -1.88, +0.73, +4.55, -5.88 and 1.16 Hz for SR1, SR2, SR3, SR4 and SR5, respectively.

[Insert Figure 1 about here]

In normal observers, L-cone cff starts to rise at about  $6.5 \log_{10}$  quanta  $s^{-1} \text{ deg}^{-2}$ , increases with a gradually decreasing slope until it approaches a plateau near 40 Hz.<sup>29, 30</sup> By contrast, the L-cone cff functions for all five CRDSR observers all show substantial losses in cff. Flicker is not detected until the mean 650-nm target radiance reaches  $8.3 \log_{10}$  quanta  $s^{-1} \text{ deg}^{-2}$ —nearly 100 times more intense than for normal observers. Thereafter, the cff increases with radiance but only up to about 30 Hz—25% lower than the normal cff.

The black dashed straight lines fitted to the mean normal and the mean CRDSR data illustrate the linear relation between cff and the logarithm of target radiance known as the Ferry-Porter law<sup>31, 32</sup>. For both the normal and affected observers, the Ferry-Porter law holds over a two and one-half log unit range. The best-fitting slopes of 8.57 and 8.51 Hz per  $\log_{10}$  unit of radiance for the normal and CRDSR observers with standard errors of 0.16 and 0.80, respectively, are very similar in the two cases. (The fitted red line will be considered in the Discussion.)

### ***L-cone modulation sensitivity***

The left-hand panel of Figure 2 shows the logarithm of temporal modulation sensitivity plotted as a function of temporal frequency (logarithmic axis) for the five CRDSR observers and the normal

comparison group averaged from data from eight observers. (Note that sensitivity, the reciprocal of threshold, increases upwards.)

[Insert Figure 2 about here]

In the mean normal observer, the L-cone modulation sensitivity is highest near 7.5 Hz and decreases at lower and higher temporal frequencies. A modulation-sensitivity function of this shape is known as a “band-pass” function. Band-pass functions are typically found in normal observers when achromatic or monochromatic flicker is used to measure sensitivity.<sup>33-38</sup> The attenuation at low temporal (and spatial) frequencies is usually attributed to surround antagonism.<sup>39-45</sup>

With the exception of the data for SR5, the L-cone modulation sensitivities for the CRDSR observers are about 1  $\log_{10}$  unit lower than those of the mean normal observer. SR5’s data are about 0.5 log units worse than the mean normal data on average, i.e., performance is about a third as good as normal. In all but one CRDSR case (SR2), however, the shapes of the modulation sensitivities functions remain approximately band-pass.

The mean CRDSR data are plotted in the upper and lower right-hand panels of Figure 2 as gray dotted symbols. To highlight the differences in shape between the normal and CRDSR data, we have replotted the individual data in the upper panel after vertically aligning them with the mean CRDSR data (using a least-squares fitting criterion). The optimal least-squared shifts of the individual data required to vertically align with the mean over the common range of frequencies was +0.06, +0.01, +0.35, -0.08 and -0.47 for SR1, SR2, SR3, SR4 and SR5, respectively. The lower right-hand panel of Figure 2 shows the differences between the mean normal and CRDSR data (black crosses) as well as the mean CRDSR data (grey dotted circles). Notice that the differences between the mean normal and CRDSR data and the mean CRDSR data themselves are relatively similar. This similarity and the continuous blue curve in the right-hand panels will be discussed subsequently.

### ***Rod critical flicker fusion***

Figure 3 shows rod cff data for the five observers affected by CRDSR plotted as a function of  $\log_{10}$  target scotopic luminance and the mean rod cff data for five observers with normal vision (green squares). The optimal least-squared shifts of the individual data required to vertically align with their mean over the common range of target luminances was +1.92, -0.57, +0.62, -0.24 and -1.72 Hz for SR1, SR2, SR3, SR4 and SR5, respectively.

[Insert Figure 3 about here]

In the mean normal observer, rod cff rises from about  $-4.0 \log_{10}$  scot. td until reaching a shallow shoulder above about  $-1.5 \log_{10}$  scot. td. The cff remains on the shallow shoulder until the cones begin to detect the target near  $-0.5 \log_{10}$  scot. td. From about  $0.5 \log_{10}$  scot. td the cff again rises steeply. The shape is fairly typical for rod cff functions (see, for example, Figure 3 of Hecht & Shlaer<sup>30</sup>). For other target sizes and wavelengths, the scotopic cff can reflect complex interactions between slow and fast rod signals<sup>46, 47</sup> or between rod signals and cones.<sup>48</sup> The rod cff functions for all five CRDSR observers all show substantial losses in cff. Comparable to the cone cff data shown in Figure 1, scotopic flicker is not detected by CRDSR observers until the mean 500-nm target is nearly 100 times more intense than the detection threshold for normal observers. The continuous red curves fitted to the CRDSR data will be discussed subsequently.

### ***S-cone critical flicker fusion***

Figure 4 shows S-cone cff data plotted as a function  $\log_{10}$  target radiance for SR1, SR2, and SR4, the only three CRDSR observers available to participate in this part of the experiment. For comparison, the mean cff data for twelve normal control observers are also plotted (dark blue squares). The optimal least-squared shifts of the individual data required to vertically align with their mean over the common range of target radiances was  $+0.51$ ,  $+2.37$ , and  $-2.88$  Hz for SR1, SR2 and SR4, respectively.

[Insert Figure 4 about here]

In the normal observer, S-cone cff rises steadily from just above a radiance of  $6.5 \log_{10}$  quanta  $s^{-1} \text{ deg}^{-2}$  until about  $9.0 \log_{10}$  quanta  $s^{-1} \text{ deg}^{-2}$ , at which it reaches a broad maximum near 22 Hz and then decreases slightly. The decrease is due, in part, to a saturation of the S-cone signal that occurs under these conditions, and also in part to chromatically-opponent interactions with the other cone types.<sup>28, 49, 50</sup> The rise in the normal cff above about  $9.9 \log_{10}$  quanta  $s^{-1} \text{ deg}^{-2}$  is due to the M-cones becoming more sensitive than S-cones and thus determining flicker detection above about  $9.9 \log_{10}$  quanta  $s^{-1} \text{ deg}^{-2}$  (see Figure 4 of Stockman & Plummer<sup>28</sup>).

As with the L-cone and rod cff data, the S-cone cff data for the CRDSR observers show considerable sensitivity losses compared to the normal data. The values for SR1 and SR4 show losses along the radiance axis of about 1  $\log_{10}$  unit and those of SR2 of about 1.5  $\log_{10}$  unit.

The black dashed lines again indicate the linear relation between cff and log radiance implied by the Ferry-Porter law. The slopes for the S-cone data are slightly shallower than for the L-cone data: The best-fitting slopes of 7.83 and 6.63 Hz per  $\log_{10}$  unit of radiance for the normal and CRDSR

observers with standard errors of 0.16 and 0.43, respectively, are, like the L-cone cff data, fairly similar in the two cases. (The red fitted curve will be discussed subsequently.)

## DISCUSSION

A consistent finding across all psychophysical measures in this study was that compared to normal observers, those affected by CRDSR suffer substantial losses in both rod- and cone-mediated visual performance.

We next quantify the extent of these sensitivity and acuity losses.

### *L-cone deficits*

The differences between the CRDSR and normal L-cone cff functions shown in Figure 1 can be quantified by shifting the normal function rightwards along the logarithmic radiance axis and displacing it vertically downwards along the linear cff axis until the normal function aligns with an individual CRDSR function. (Note that horizontally shifting the template along the *logarithmic* radiance axis is equivalent to scaling the radiance.) To facilitate these alignments, we derived an arbitrary polynomial template, to describe the normal data and shown in Figure 1 as the dark red line passing through the red squares.

**TABLE 1**

	Vertical linear shift in cff (Hz)	Horizontal logarithmic shift	$R^2$
L-cone	4.62±3.74	1.28±0.38	0.72
Rods	4.59±0.59	1.09±0.16	0.40
S-cone	3.04±0.90	0.86±0.15	0.79
Mean	4.05	1.08	

The fit to the CRDSR data was carried out by shifting the template using a least-squares fitting criterion to fit all the *unshifted* CRDSR data (as plotted in Figure 1). The mean best-fitting values and ± the standard error of the two shifts are given in Table 1 (L-cone row). The fit has an  $R^2$  of 0.72 (relative to the unshifted individual data). The best-fit shown by the solid red curve is the template

polynomial shifted rightwards by  $1.28 \pm 0.38 \log_{10}$  unit (a scaling of 19.05) and shifted down by  $4.62 \pm 3.74$  Hz. These mainly descriptive values are difficult to relate to the underlying physiology without making speculative assumptions, but they do allow us to quantify the losses of the CRDSR observers.

A clear conclusion from the fit is that the 650-nm target is much less effective for the CRDSR observers than for the normal observer by over an order of magnitude. The interpretation of the vertical shift in cff, and the extent to which it can be considered as independent from the horizontal logarithmic shift (given its high standard error), is more equivocal. The inclusion of a linear shift in the model allows us to apply a metric developed in the Appendix of a companion paper on enhanced S-cone syndrome<sup>51</sup> that translates vertical shifts in cff to changes in photoreceptor number (for targets of between  $2.98^\circ$  and  $7.10^\circ$  in diameter). The metric is based on (i) a useful approximation, known as the Granit-Harper law: that the cff increases linearly with the logarithm of the target area,<sup>52, 53</sup> (ii) cff data from Kugelmass & Landis<sup>54</sup> measured as a function of target area and luminance, and (iii) human cone density measurements that link target area and cone number made by Curcio et al.<sup>55</sup> It equates the changes in cone number caused by changing target area with changes in cone number caused by photoreceptor gain or loss *within* a fixed target area and provides a crude guide to photoreceptor loss.

For a change in cff of  $\Delta\text{cff}$  Hz, the relative change,  $r$ , in the number of cones:

$$r = 10^{\frac{\Delta\text{cff}}{5.93}}. \quad [3]$$

Using Equation [3], we can calculate from the decrease in cff the factor by which  $r$  changes. According to Equation [3], the decline in cff of 4.53 Hz in CRDSR observers is caused by a decrease in the number of cones by a factor of 5.81. We emphasize that this is a speculative approximation, but it provides a rough estimate of the changes caused by CRDSR. There are cone density measurements using adaptive optics scanning laser ophthalmoscopy (AOSLO) against which we can compare this estimate. In three observers with CRDSR, AOSLO reductions in cone density of about 3, 9 and 19 times were found (see p. 910 of Vincent et al.<sup>13</sup>).

Another way of comparing cff data of the normal and affected observers is to consider the slopes of the cff *versus* log radiance functions where the Ferry-Porter law holds. Some have suggested that this slope can be directly related to the limiting properties of the underlying unadapted cone photoreceptor response (see, in particular, Tyler & Hamer<sup>56</sup>). However, it seems more likely—at least for central vision—that the Ferry-Porter slopes reflect the convolution of the properties of the underlying photoreceptor response and those of adapting stages—some of which are probably within the photoreceptor (see, for example, Stockman et al.<sup>57</sup>). Nevertheless,

according to both views, the Ferry-Porter law slopes can, at least in principle, be linked to the underlying photoreceptor responses. The similarities between the mean Ferry-Porter law L-cone cff slopes in Hz per decade of radiance for normals ( $8.57 \pm 0.16$ ) and affected observers ( $8.51 \pm 0.80$ ) suggests that the initial L-cone photoreceptor response is relatively unaffected in the disease, and supports the proposal<sup>6-8</sup> that the deficit arises after the transduction cascade, but before the inner nuclear layer.

As noted above, the voltage-gated potassium subunit encoded by the *KCNV2* gene is important for shaping the photoreceptor output response and setting the resting potential.<sup>19</sup> The differences between the shapes of the CRDSR and mean normal temporal contrast sensitivity functions shown in Figure 2 provide clues about precisely how the defect alters the visual response. For instance, the differences between the normal and CRDSR functions are not obviously due to changes in the effective adaptation level. Such changes would have the effect of shortening or lengthening the time constants of low-pass stages contributing to the visual response (see upper panels of Figure 6 of Stockman et al.<sup>57</sup>) rather than the changes seen in Figure 2. Instead, the CRDSR data can be reasonably well accounted for simply by halving the normal logarithmic modulation sensitivities as shown by the blue curves (which is equivalent to taking the square-root of the linear sensitivities). As a result, not only are the CRDSR data similar to a halving of the normal logarithmic modulation sensitivities, but so too are the logarithmic *differences* between the mean normal and CRDSR data as illustrated by the crosses in the lower right-hand panel of Figure 2.

This compression of the CRDSR temporal contrast sensitivity function is consistent with the defect in the voltage-gated potassium channel causing a nonlinear distortion of the visual signal in the CRDSR observer. One possibility is that the defect causes the photoreceptor to have an expansively nonlinear input-output function, such that the output is relatively depressed at low inputs but grows with the square of the input (rather than linearly as in the normal observer). As a result, the CRDSR modulation sensitivity functions will be compressed relative to the normal functions in the way that we find. If the input-output function continues to be expansive up to high input levels, it could also account for the supernormal ERG amplitudes found with intense scotopic flashes. For our psychophysical measurements, however, the thresholds for the CRDSR observers always fall below those of normal observers, which suggests that output of the putative expansively nonlinear input-output function in the CRDSR observers never exceeds that of the normal input-output function under the conditions we tested.

The fact that the relationship between the logarithmic mean sensitivities is consistent with a simple halving of the normal (logarithmic) function, suggests that underlying the distortion of the visual signal in the CRDSR observer, other aspects of visual processing, such as lateral inhibition and

adaptation-dependent changes in modulation sensitivity in the transduction cascade (see, for discussion, Stockman et al.<sup>57</sup>) are relatively normal.

There are other interpretations of the differences between the CRDSR and normal temporal contrast sensitivity functions. Another possibility is that the defect in the voltage-gated potassium channel, rather than making the input-output function expansively nonlinear, might result in receptor signalling becoming much noisier. If noise with equal variance from a number of uncorrelated and uninformative channels affects the cone signal, there would be a loss in signal-to-noise ratio that would decline as the square-root of the number of uninformative channels.<sup>58</sup> This decline would cause a compression of the temporal contrast sensitivity function comparable to the one that we find.

### ***Scotopic (rod) deficits***

Like the L-cone data, the differences between the CRDSR and normal rod cff functions shown in Figure 3 can be approximated by a horizontal displacement of the normal function along the logarithmic radiance axis and a vertical displacement along the cff axis. Again, to facilitate these approximations, we have derived an arbitrary polynomial template, shown, in Figure 3, by the black line through the normal data points (green squares).

As for the L-cone cff data, the fit to the CRDSR rod data was carried out by shifting the template using a least-squares fitting criterion to fit all the *unshifted* CRDSR data (as plotted in Figure 3). The best-fitting values and  $\pm$  the standard error of each parameter are given in Table 1 (row labelled Rods). The best-fit shown by the solid red curve is the template polynomial shifted rightwards  $1.09 \pm 0.16 \log_{10}$  unit (a scaling of 12.30) and shifted vertically by  $4.59 \pm 0.59$  Hz. The fit has an  $R^2$  of 0.40 (relative to the unshifted individual data).

The fits suggest that the 500 nm target is 12.30 times less effective for the CRDSR observers. The need for a vertical shift in cff is much more apparent in these data because of the shoulder in the cff function. Using Equation [3], this suggests a decrease in photoreceptor number by a factor of 5.94.

Note that for both fits, the best-fitting scotopic values are similar in magnitude to those for the L-cone fits, which suggests that the rod and cone losses in this disease are also of a comparable magnitude.

The lowest target luminance at which flicker of any frequency can be seen for our CRDSR observers is about 100 times higher than for normal observers, which is consistent with other quantified reports of rod sensitivity losses.<sup>6-8</sup> Yet many other clinical evaluations of CRDSR

observers<sup>9, 12</sup> report observers without night blindness. The results of Figure 3, show clearly that any diagnosis of night blindness in CRDSR affected patients is likely to be equivocal, because the degree of 'night blindness' depends very much on the lighting conditions. Below about  $-2 \log_{10} \text{scot. td}$  our 5 observers were effectively "night blind", but above that level some rod response could be measured in all of them.

### ***S-cone deficits***

The differences between the CRDSR and normal S-cone cff functions shown in Figure 4 can also be approximated by a horizontal displacement of the normal function along the radiance axis and a vertical displacement along the cff axis. As before, we derived an arbitrary polynomial template, shown, in Figure 4, by the black line passing through the normal data points (blue squares).

As for the L-cone and rod cff data, the fit to the CRDSR S-cone data was carried out by shifting the template using a least-squares fitting criterion to fit all the *unshifted* CRDSR data (as plotted in Figure 4). The best-fitting values and  $\pm$  the standard error of each parameter are given in Table 1 (S-cone row). The best-fit shown by the solid red curve is the template polynomial shifted rightwards  $0.86 \pm 0.15 \log_{10}$  unit (a scaling of 7.24) and shifted vertically by  $3.04 \pm 0.90$  Hz. The fit has an  $R^2$  of 0.79 (relative to the unshifted individual data).

The fits suggest that the 440 nm target is 7.24 times less effective for the CRDSR observers. Using Equation [3], this suggests a mean decrease in cone number by a factor of 3.26. Contrary to previous suggestions,<sup>1, 10</sup> the S-cones in our observers appear to be also affected by this disease.

Like the L-cone cff data, the mean Ferry-Porter law S-cone cff slopes in Hz per decade of radiance for normals ( $7.83 \pm 0.16$ ) and affected observers ( $6.63 \pm 0.43$ ) are fairly similar, which suggests that the initial S-cone photoreceptor response is relatively unaffected in the disease.

### ***Conclusions***

The losses in temporal acuity caused by CRDSR are roughly equivalent for vision mediated by rods, L-cones and S-cones. Our analyses show that relative to the normal cff data the mean shifts in the CRDSR data are a rightward logarithmic shift of  $1.08 \log_{10}$  unit along the radiance or luminance scale (which is equivalent to a scaling of about 12) and a downward shift of 4.05 Hz along the cff scale. The rightward scaling differs by no more than a factor of 2.63 between photoreceptor types and the downward shift by a factor of 1.51. However, the Ferry-Porter slopes for the L-cone and S-

cone cff data are similar, which suggests that the cone photoreceptor responses may be relatively unaffected by the disease.

The changes in temporal contrast-sensitivity are broadly consistent with the defect in the voltage-gated potassium channel producing either a nonlinear distortion of the photoreceptor response or perhaps an increase in transmission noise.

Under the conditions of our experiments, the gain in rod function suggested by the supernormal scotopic ERG seems to be related to no observable benefit in vision mediated by rods. Measures of temporal contrast sensitivity suggest the possibility that the deficit in the voltage-gated potassium channel results in a nonlinear expansive distortion of the signals from the surviving cone photoreceptors. The name of the disorder is indeed a misnomer,<sup>9</sup> mainly because it underemphasizes the associated rod dysfunction.

## ACKNOWLEDGEMENTS

This work was supported by grants from Fight for Sight, BBSRC, EPSRC and the National Institute for Health Research Biomedical Research Centre at Moorfields Eye Hospital NHS Foundation Trust and UCL Institute of Ophthalmology. ARW and ATM are supported a Foundation for Fighting Blindness Research Center grant for the Study of Retinal Degenerative Diseases. MM is supported by a Foundation Fighting Blindness Career Development Award. We especially acknowledge the help of the observers who participated in this study without whom this work would not have been possible.

## REFERENCES

1. Gouras P, Eggers HM, MacKay CJ. Cone dystrophy, nyctalopia, and supernormal rod responses. A new retinal degeneration. *Archives of Ophthalmology* 1983;101:718-724.
2. Alexander KR, Fishman GA. Supernormal scotopic ERG in cone dystrophy. *British Journal of Ophthalmology* 1984;68:69-78.
3. Yagasaki K, Miyake Y, Litao RE, Ichikawa K. Two cases of retinal degeneration with an unusual form of electroretinogram. *Documenta Ophthalmologica* 1986;63:73-82.

4. Foerster MH, Kellner U, Wessing A. Cone dystrophy and supernormal dark-adapted b-waves in the electroretinogram. *Graefes Archives of Clinical and Experimental Ophthalmology* 1990;228:116-119.
5. Sandberg MA, Miller S, Berson EL. Rod electroretinograms in an elevated cyclic guanosine monophosphate-type human retinal degeneration. Comparison with retinitis pigmentosa. *Investigative Ophthalmology and Visual Science* 1990;31:228-2287.
6. Kato M, Kobayashi R, Watanabe I. Cone dysfunction and supernormal scotopic electroretinogram with a high-intensity stimulus. A report of three cases. *Documenta Ophthalmologica* 1993;84:71-81.
7. Rosenberg T, Simonsen SE. Retinal cone dysfunction of supernormal rod ERG type. Five new cases. *Acta Ophthalmologica* 1993;71:246-255.
8. Hood DC, Cideciyan AV, Halevy DA, Jacobsen SG. Sites of disease action in a retinal dystrophy with supernormal and delayed rod electroretinogram b-waves. *Vision Research* 1996;36:889-901.
9. Robson AG, Webster AR, Michaelides M, et al. Cone dystrophy with supernormal rod electroretinogram: a comprehensive genotype/phenotype study including fundus autofluorescence and extensive electrophysiology. *Retina, the journal of retinal and vitreous diseases* 2010;30:51-62.
10. Michaelides M, Holder GE, Webster AR, et al. A detailed phenotypic study of "cone dystrophy with supernormal rod ERG". *British Journal of Ophthalmology* 2005;89:332-339.
11. Wissinger B, Dangel S, Jägle H, et al. Cone dystrophy with supernormal rod response is strictly associated with mutations in KCNV2. *Investigative Ophthalmology and Visual Science* 2008;49:751-757.
12. Zobor D, Kohl S, Wissinger B, Zrenner E, Jägle H. Rod and cone function in patients with KCNV2 retinopathy. *Plos One* 2012;7:e46762.
13. Vincent A, Wright T, Garcia-Sanchez Y, et al. Phenotypic characteristics including in vivo cone photoreceptor mosaic in KCNV2-related "cone dystrophy with supernormal rod electroretinogram". *Investigative Ophthalmology and Visual Science* 2013;54:898-908.
14. Hood DC, Birch DG. The a-wave of the human ERG and rod receptor function. *Investigative Ophthalmology and Visual Science* 1990;31:2070-2081.
15. Hood DC, Birch DG. Light adaptation of the human rod receptors: the leading edge of the human a-wave and models of rod receptor activity. *Vision Research* 1993;33:1605-1618.

16. Wu H, Cowing JA, Michaelides M, et al. Mutations in the gene *KCNV2* encoding a voltage-gated Potassium channel subunit cause "cone dystrophy with supernormal rod electroretinogram" in humans. *American Journal of Human Genetics* 2006;79:574-579.
17. Thiagalingam S, McGee TL, Sandberg MA, Trzuppek KM, Berson EL, Dryja TP. Novel mutations in the *KCNV2* gene in patients with cone dystrophy and a supernormal rod electroretinogram. *Ophthalmic Genetics* 2007;28:135-142.
18. Salah SB, Kamei S, Sénéchal A, et al. Novel *KCNV2* mutations in cone dystrophy with supernormal rod electroretinogram. *American Journal of Ophthalmology* 2008;145:1099-1106.
19. Barnes S. After transduction: Response shaping and control of transmission by ion channels of the photoreceptor inner segment. *Neuroscience* 1994;58:447-459.
20. Stockman A, Langendörfer M, Sharpe LT. Light adaptation and the human temporal response. *Invest Ophth Vis Sci* 1998;39:S1109.
21. Stockman A, Smithson HE, Webster AR, et al. The loss of the PDE6 deactivating enzyme, RGS9, results in precocious light adaptation at low light levels. *Journal of Vision* 2008;8:10.11-10.
22. Stockman A, Smithson HE, Michaelides M, Moore AT, Webster AR, Sharpe LT. Residual cone vision without  $\alpha$ -transducin. *Journal of Vision* 2007;7:8.1-13.
23. Stockman A, Sharpe LT, Tufail A, Kell PD, Ripamonti C, Jeffery G. The effect of sildenafil citrate (Viagra®) on visual sensitivity. *Journal of Vision* 2007;7(8):4:4, 1-15.
24. Kohlrausch A. Untersuchungen mit farbigen Schwellprüflichtern über den Dunkeladaptationsverlauf des normalen Auges. *Pflügers Archiv für die Gesamte Physiologie des Menschen und der Tiere* 1922;196:113-117.
25. Hecht S, Haig C, Wald G. The dark adaptation of retinal fields of different size and location. *Journal of General Physiology* 1935;19:321-337.
26. Stockman A, MacLeod DIA, Lebrun S. Faster than the eye can see: blue cones respond to rapid flicker. *Journal of the Optical Society of America A* 1993;10:1396-1402.
27. Stockman A, MacLeod DIA, DePriest DD. The temporal properties of the human short-wave photoreceptors and their associated pathways. *Vision Research* 1991;31:189-208.
28. Stockman A, Plummer DJ. Color from invisible flicker: a failure of the Talbot-Plateau law caused by an early "hard" saturating nonlinearity used to partition the human short-wave cone pathway. *Vision Research* 1998;38:3703-3728.
29. Hecht S, Verriyp CD. The influence of intensity, color and retinal location on the fusion frequency of intermittent illumination. *Proceedings of the National Academy of Sciences of the United States of America* 1933;19:522-535.

30. Hecht S, Schlaer S. Intermittent stimulation by light. V. The relation between intensity and critical frequency for different parts of the spectrum. *Journal of General Physiology* 1936;19:965-977.
31. Ferry J. Persistence of vision. *American Journal of Science and Arts* 1892;44:192-207.
32. Porter TC. Contributions to the study of flicker. II. *Proceedings of the Royal Society of London Series A* 1902;70:313-319.
33. De Lange H. Research into the dynamic nature of the human fovea-cortex systems with intermittent and modulated light. I. Attenuation characteristics with white and colored light. *Journal of the Optical Society of America* 1958;48:777-784.
34. Kelly DH. Visual responses to time-dependent stimuli I. Amplitude sensitivity measurements. *Journal of the Optical Society of America* 1961;51:422-429.
35. Roufs JAJ. Dynamic properties of vision-I. Experimental relationships between flicker and flash thresholds. *Vision Research* 1972;12:261-278.
36. Green DG. Sinusoidal flicker characteristics of the colour-sensitive mechanisms of the eye. *Vision Research* 1969;9:591-601.
37. Kelly DH. Lateral inhibition in human colour mechanisms. *Journal of Physiology* 1973;228:55-72.
38. Varner D, Jameson D, Hurvich LM. Temporal sensitivities related to colour theory. *Journal of the Optical Society of America A* 1984; 1:474-481.
39. Schober HAW, Hilz R. Contrast sensitivity of the human eye for square-wave gratings. *Journal of the Optical Society of America* 1965;55:1086-1091.
40. Robson JG. Spatial and temporal contrast sensitivity functions of the visual system. *Journal of the Optical Society of America* 1966;56:1141-1142.
41. Nachmias J. Effect of exposure duration on visual contrast sensitivity with square-wave gratings. *Journal of the Optical Society of America* 1967;57:421-427.
42. Ratliff F, Knight BW, Toyoda J-I, Hartline HK. Enhancement of flicker by lateral inhibition. *Science* 1967;158:392-393.
43. Kelly DH. Flickering patterns and lateral inhibition. *Journal of the Optical Society of America* 1969;59:1361-1370.
44. Ratliff F, Knight BW, Graham N. On tuning and amplification by lateral inhibition. *Proceedings of the National Academy of Science USA* 1969;62:733-740.
45. Watson AB. Temporal sensitivity. In: Boff K, Kaufman L, Thomas J (eds), *Handbook of Perception and Human Performance*. New York: Wiley; 1986:6-1-6-43.
46. Conner JD, MacLeod DIA. Rod photoreceptors detect rapid flicker. *Science* 1977;195:689-699.

47. Stockman A, Sharpe LT, MacLeod DIA. A duality of rod flicker detection:  $\pi_0$  and  $\pi_0'$ . *Invest Ophthalmol Vis Sci* 1988;29:91.
48. MacLeod DIA. Rods cancel cones in flicker. *Nature* 1972;235:173-174.
49. Mollon JD, Polden PG. Saturation of a retinal cone mechanism. *Nature* 1977;259:243-246.
50. Stromeyer CF, III, Kronauer RE, Madsen JC. Response saturation of short-wavelength cone pathways controlled by color-opponent mechanisms. *Vision Research* 1979;19:1025-1040.
51. Ripamonti C, Aboshiha J, Henning GB, et al. Vision in observers with enhanced S-cone syndrome: an excess of S-cones connected to conventional S-cone pathways and a faster pathway. submitted.
52. Granit R, Harper P. Comparative studies on the peripheral and central retina. II. Synaptic reactions in the eye. *American Journal of Physiology* 1930;95:211-228.
53. Hecht S, Smith EL. Intermittent stimulation by light. VI. Area and the relation between critical frequency and intensity. *Journal of General Physiology* 1936;19:979-989.
54. Kugelmass S, Landis C. The Relation of Area and Luminance to the Threshold for Critical Flicker Fusion. *American Journal of Psychology* 1955;68:1-19.
55. Curcio CA, Sloan KR, Kalina RE, Hendrickson AE. Human photoreceptor topography. *Journal of Comparative Neurology* 1990;292:497-523.
56. Tyler CW, Hamer RD. Analysis of visual modulation sensitivity. IV. Validity of the Ferry-Porter law. *Journal of the Optical Society of America A* 1990;7:743-758.
57. Stockman A, Langendörfer M, Smithson HE, Sharpe LT. Human cone light adaptation: from behavioral measurements to molecular mechanisms. *Journal of Vision* 2006;6:1194-1213.
58. Green DM, Swets JA. *Signal detection theory and psychophysics*. New York: Wiley; 1966.

## FIGURE LEGENDS

**Figure 1.** L-cone critical flicker fusion frequencies (linear scale) measured on a 481-nm background of  $8.26 \log_{10}$  quanta  $s^{-1} \text{ deg}^{-2}$  are plotted as a function of the mean  $\log_{10}$  radiance of a 650-nm flickering target. Data are plotted for five CRDSR observers: SR1 (blue triangles), SR2 (purple inverted triangles), SR3 (green diamonds), SR4 (yellow circles) and SR5 (orange hexagons). The mean CRDSR data (gray dotted circles) and mean data for 12 normal observers (dark red squares) are also shown. The dark red line through the red squares provides a template for the normal data. The red line is a shifted version of this template as described in the text. The error bars are  $\pm 1$  standard error of the mean (s.e.m.) within observers for the individual CRDSR data, and between observers for the mean

data. The dashed black lines are best-fitting linear slopes fitted to the mean data for normals and affected observer over the range of radiances over which the Ferry-Porter law holds (see text for details). The best-fitting slopes are 8.6 Hz per decade for normals and 8.5 Hz per decade for the CRDSR observers.

**Figure 2.** Left-hand panel:  $\log_{10}$  L-cone modulation sensitivities measured using a sinusoidally modulated 650-nm target fixed at a radiance of  $10.28 \log_{10} \text{ quanta s}^{-1} \text{ deg}^{-2}$  superimposed on a 480-nm background of  $8.29 \log_{10} \text{ quanta s}^{-1} \text{ deg}^{-2}$  ( $1.42 \log_{10}$  photopic trolands or  $2.58 \log_{10}$  scotopic trolands) are plotted as a function of temporal frequency (logarithmic axis). Data are plotted for the five CRDSR observers: SR1 (blue triangles), SR2 (purple inverted triangles), SR3 (green diamonds), SR4 (yellow circles) and SR5 (orange hexagons). The mean data for 8 normal observers (red squares) are also shown. Upper-right-hand panel: The  $\log_{10}$  L-cone modulation sensitivities for the individual CRDSR observers vertically aligned using a least-squares fitting procedure with the mean CRDSR data (grey dotted circles). The logarithmic mean normal data are replotted as in the left-hand panel (red squares) but also divided by two (blue line). Lower-right-hand panel: The logarithmic mean normal data divided by two (blue line) compared with the differences between the mean normal and CRDSR data (black crosses). The error bars in all figures are  $\pm 1$  standard error of the mean (s.e.m.) within observers for the individual CRDSR data, and between observers for the mean data.

**Figure 3.** Rod critical fusion frequencies (linear scale) measured at  $10^\circ$  in the temporal retina are plotted as a function of the mean  $\log_{10}$  scotopic luminance of the 500-nm flickering target. Individual data are plotted for the five CRDSR observers: SR1 (blue triangles), SR2 (purple inverted triangles), SR3 (green diamonds), SR4 (yellow circles) and SR5 (orange hexagons). The mean CRDSR data (grey dotted circles) and mean data for 5 normal observers (green squares) are also shown. The black curve through the green squares provides a template for the normal data. The red line is a shifted version of this template as described in the text. The error bars are  $\pm 1$  standard error of the mean (s.e.m.) within observers for the individual CRDSR data, and between observers for the mean data.

**Figure 4.** S-cone critical flicker fusion frequencies measured on a 620-nm background of  $11.41 \log_{10} \text{ quanta s}^{-1} \text{ deg}^{-2}$  are plotted as a function of the mean log radiance of the 440-nm flickering target. Only three CRDSR observers participated in this experiment: SR1 (blue triangles), SR2 (purple inverted triangles) and SR4 (yellow circles). The mean CRDSR data (grey dotted circles) and the mean data for 12 normal observers (dark blue squares) are also shown. The continuous blue curve

through the dark blue squares provides a template for the normal data. The red line is a shifted scaled version of this template as described in the text. The error bars are  $\pm 1$  standard error of the mean (s.e.m.) within observers for the individual CRDSR data, and between observers for the mean data. The dashed black lines are best-fitting linear slopes fitted to the mean data for normals and affected observer over the range of radiances over which the Ferry-Porter law holds. The best-fitting slopes are 7.8 Hz per decade for normals and 6.6 Hz per decade for the CRDSR observers.

## TABLE LEGEND

**Table 1.** Best-fitting linear and logarithmic shifts for the L-cone, rod and S-cone cff data (see text for details).

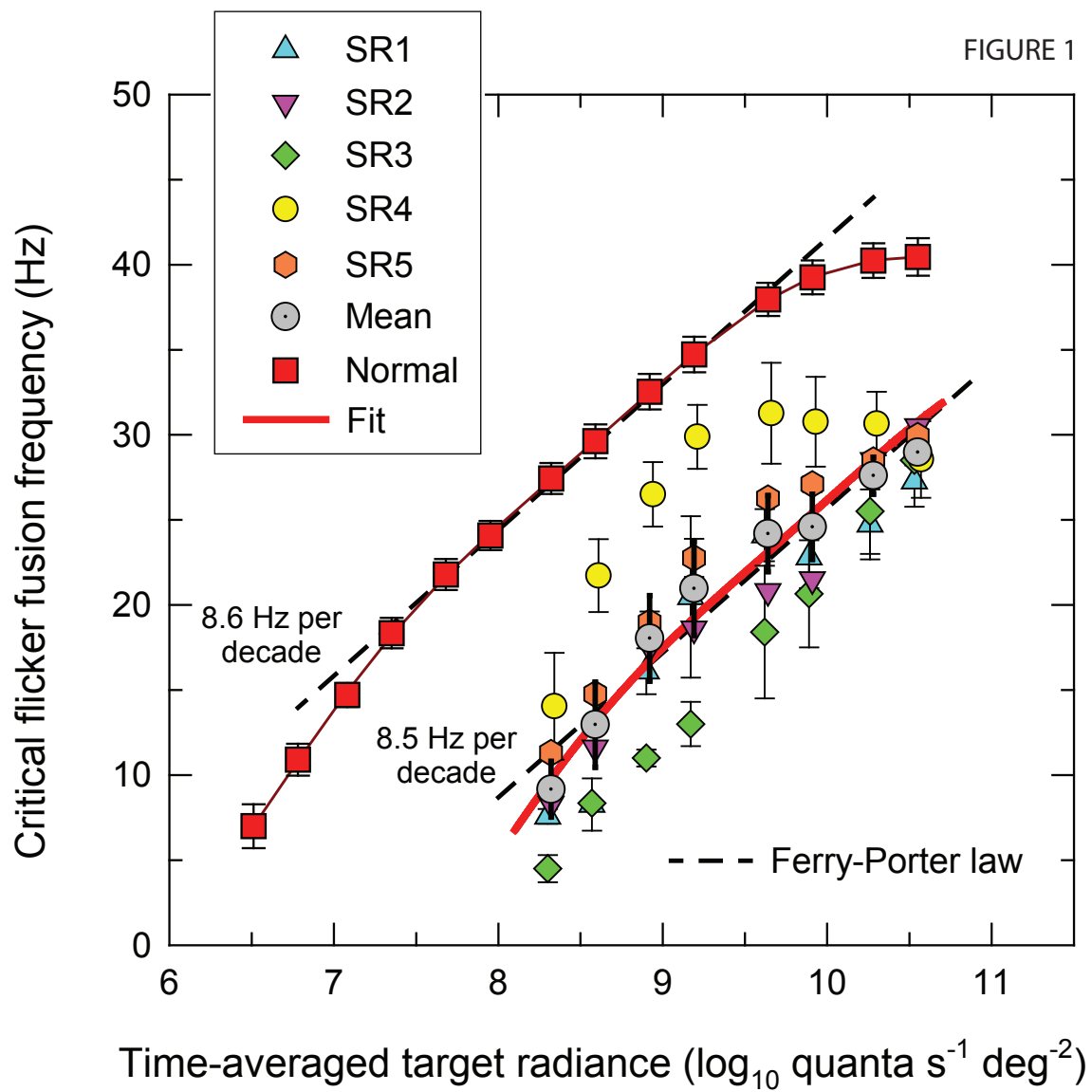




FIGURE 3

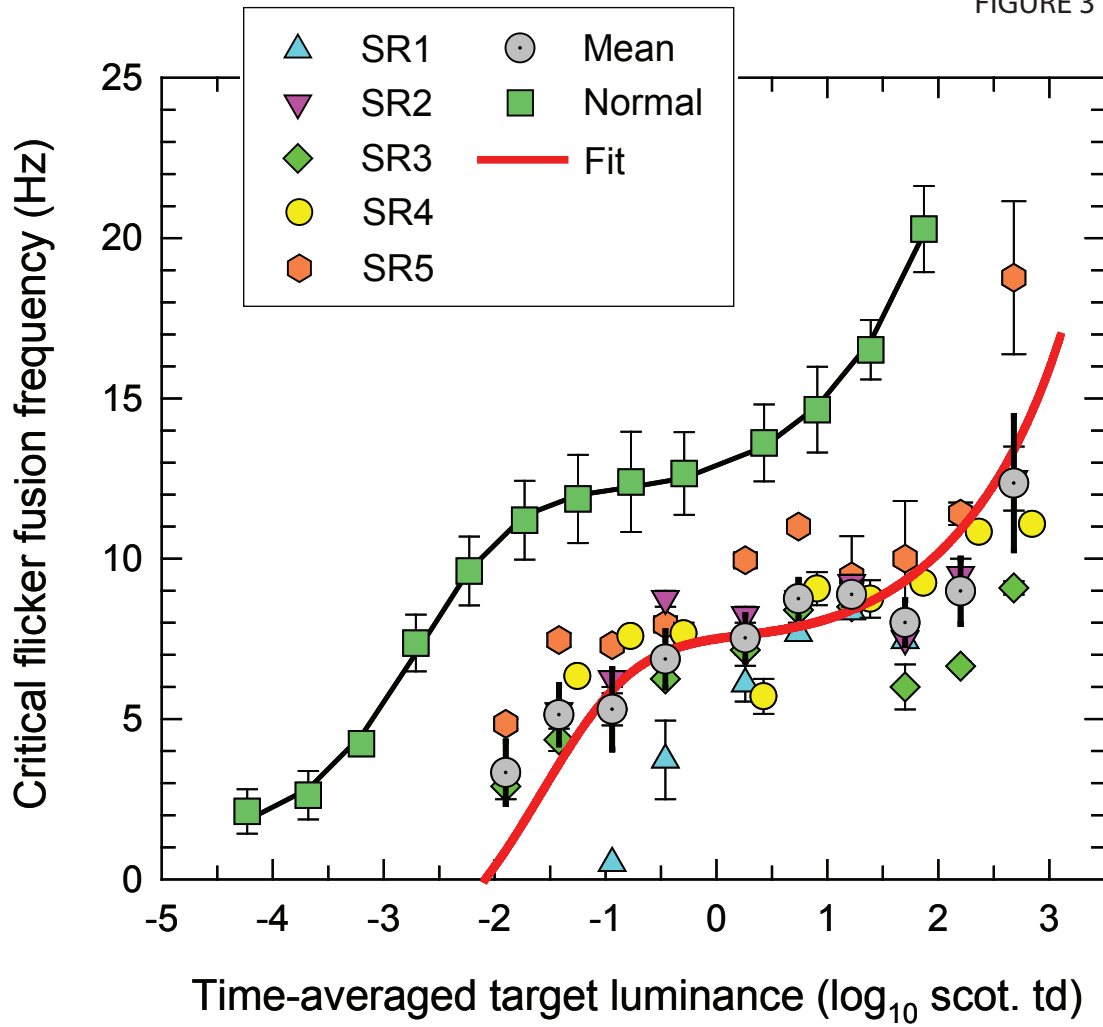


FIGURE 4

